Two-dimensional, homogeneous, isotropic fluid turbulence with polymer additives

Anupam Gupta,[1,*] Prasad Perlekar,[2,†] and Rahul Pandit[2,‡]

[1] *Centre for Condensed Matter Theory, Department of Physics, Indian Institute of Science, Bangalore 560012, India.*

[2] *Department of Physics, Department of Mathematics and Computer Science, Technische Universiteit Eindhoven, Eindhoven, The Netherlands.*

We present the most extensive direct numerical simulations. attempted so far, of statistically steady, homogeneous, isotropic turbulence in two-dimensional fluid films with air-drag-induced friction and with polymer additives. Our study reveals that the polymers (a) reduce the total fluid energy, enstrophy, and palinstrophy, (b) modify the fluid energy spectrum both in inverse- and forward-cascade régimes, (c) reduce small-scale intermittency, (d) suppress regions of large vorticity and strain rate and (e) stretch in strain-dominated regions. We compare our results with the earlier experimental studies; and we propose new experiments.

PACS numbers: 47.27.Gs, 47.27.Ak

Polymer additives have remarkable effects on turbulent flows: in wall-bounded flows they lead to the dramatic phenomenon of drag reduction [1, 2]; in homogeneous, isotropic turbulence they give rise to dissipation reduction, a modification of the energy spectrum, and a suppression of small-scale structures [3–8]. These effects have been studied principally in three-dimensional (3D) flows; their two-dimensional (2D) analogs have been studied only over the past decade in experiments [11, 13] on and direct numerical simulations (DNSs) [14] of fluid films with polymer additives. It is important to investigate the differences, both qualitative and quantitative, between 2D and 3D fluid turbulence with polymer additives because the statistical properties of fluid turbulence in 2D and 3D are qualitatively different [16]: the inviscid, unforced 2D Navier-Stokes (NS) equation admits more conserved quantities than its 3D counterpart; one consequence of this is that the energy spectrum for 2D fluid turbulence displays an *inverse* cascade of energy, from the energy-injection length scale l_{inj} to larger length scales, and a *forward* cascade of enstrophy, from l_{inj} to smaller length scales. We have, therefore, carried out the most extensive and high-resolution DNS studies, attempted so far, of homogeneous, isotropic turbulence in the incompressible, 2D NS equation with air-drag-induced friction and polymer additives, which we model by using the finitely-extensible-nonlinear-elastic-Peterlin (FENE-P) model for the polymer-conformation tensor. Our study yields several interesting results that we summarize below. We find that the inverse-cascade part of the energy spectrum in 2D fluid turbulence is suppressed by the addition of polymers. The effect of polymers on the forward-cascade part of the fluid energy spectrum in 2D is similar to their effect on the energy spectrum in 3D fluid turbulence; in particular, there is slight reduction at intermediate wave-number and significant enhancement of the fluid energy spectrum in the large-wave-number range. In addition, we find clear manifestations of dissipation-reduction-type phenomena [6, 7]: the addition of polymers to the turbulent 2D fluid leads to a reduction of the total energy, and energy- and enstrophy-dissipation rates, a suppression of small-scale intermittency, and a decrease in high-intensity vortical and strain-dominated regimes. We show that the probability distribution functions (PDFs) of σ^2 and ω^2, the squares of the strain rate and the vorticity, respectively, agree qualitatively with those obtained in experiments [13]. We also present PDFs of the Okubo-Weiss parameter $\Lambda = (\omega^2 - \sigma^2)/8$, whose sign determines whether the flow in a given region is vortical or strain-dominated [10, 15], and PDFs of the polymer extension; and we show that polymers stretch preferentially in strain-dominated regions.

The 2D incompressible NS and FENE-P equations can be written in terms of the stream-function ψ and the vorticity $\boldsymbol{\omega} = \nabla \times \mathbf{u}(\mathbf{x}, t)$, where $\mathbf{u} \equiv (-\partial_y\psi, \partial_x\psi)$ is the fluid velocity at the point $\mathbf{x}$ and time t, as follows:

$$D_t\omega = \nu\nabla^2\omega + \frac{\mu}{\tau_P}\nabla \times \nabla.[f(r_P)\mathcal{C}] - \alpha\omega + F_\omega; \quad (1)$$

$$\nabla^2\psi = \omega; \quad (2)$$

$$D_t\mathcal{C} = \mathcal{C}.(\nabla\mathbf{u}) + (\nabla\mathbf{u})^T.\mathcal{C} - \frac{f(r_P)\mathcal{C} - \mathcal{I}}{\tau_P}. \quad (3)$$

Here $D_t \equiv \partial_t + \mathbf{u}.\nabla$, the uniform solvent density $\rho = 1$, α is the coefficient of the friction, ν the kinematic viscosity of the fluid, μ the viscosity parameter for the solute (FENE-P), and τ_P the polymer relaxation time; to mimic soap-film experiments [13] we use a Kolmogorov-type forcing $F_\omega \equiv k_{inj}F_0\cos(k_{inj}y)$, with amplitude F_0; the energy-injection wave vector is k_{inj} (the length scale $l_{inj} \equiv 2\pi/k_{inj}$); the superscript T denotes a transpose, $\mathcal{C}_{\beta\gamma} \equiv \langle R_\beta R_\gamma\rangle$ are the elements of the polymer-conformation tensor (angular brackets indicate an average over polymer configurations), the identity tensor $\mathcal{I}$ has the elements $\delta_{\beta\gamma}$, $f(r_P) \equiv (L^2 - 2)/(L^2 - r_P^2)$ is the FENE-P potential that ensures finite extensibility of the polymers, and $r_P \equiv \sqrt{\mathrm{Tr}(\mathcal{C})}$ and L are, respectively, the length and the maximal possible extension of the poly-

mers; and $c \equiv \mu/(\nu+\mu)$ is a dimensionless measure of the polymer concentration [18] .

We have developed a parallel MPI code for our DNS, which uses periodic boundary conditions because we study homogeneous, isotropic, turbulence; our square simulation domain has side $\mathbb{L} = 2\pi$ and N^2 collocation points. We use a fourth-order Runge-Kutta scheme, with time step δt, for time marching and an explicit, fourth-order, central-finite-difference scheme in space and the Kurganov-Tadmor (KT) shock-capturing scheme [17] for the advection term in Eq. (3); the KT scheme (see Eq. (7) of Ref. [7]) resolves sharp gradients in $\mathcal{C}_{\beta\gamma}$ and thus minimizes dispersion errors, which increase with L and τ_P. We solve Eq. (2) in Fourier space by using the FFTW library [19]. We choose $\delta t \simeq 5\times10^{-4}$ to 5×10^{-5} so that r_P does not become larger than L. Table I lists the parameters we use. We preserve the symmetric-positive-definite (SPD) nature of $\mathcal{C}$ at all times by adapting to two dimensions the Cholesky-decomposition scheme of Refs. [6, 7, 18]. In particular, we define $\mathcal{J} \equiv f(r_P)\mathcal{C}$, so Eq. (3) becomes

$$D_t\mathcal{J} = \mathcal{J}.(\nabla\mathbf{u}) + (\nabla\mathbf{u})^T.\mathcal{J} - s(\mathcal{J}-\mathcal{I}) + q\mathcal{J}, \qquad (4)$$

where $s = (L^2-2+j^2)/(\tau_P L^2)$, $q = [d/(L^2-2) - (L^2-2+j^2)(j^2-2)/(\tau_P L^2(L^2-2))]$, $j^2 \equiv Tr(\mathcal{J})$, and $d = Tr[\mathcal{J}.(\nabla\mathbf{u}) + (\nabla\mathbf{u})^T.\mathcal{J}]$. Given that $\mathcal{C}$ and hence $\mathcal{J}$ are SPD matrices, we can write $\mathcal{J} = \mathcal{L}\mathcal{L}^T$, where $\mathcal{L}$ is a lower-triangular matrix with elements ℓ_{ij}, such that $\ell_{ij} = 0$ for $j > i$; Eq.(4) now yields ($1 \le i \le 2$ and $\Gamma_{ij} \equiv \partial_i u_j$)

$$\begin{aligned}
D_t\ell_{11} &= \Gamma_{11}\ell_{11} + \Gamma_{21}\ell_{21} + \frac{1}{2}\Big[(q-s)\ell_{11} + \frac{s}{\ell_{11}}\Big],\\
D_t\ell_{21} &= \Gamma_{12}\ell_{11} + \Gamma_{21}\frac{\ell_{22}^2}{\ell_{11}} + \Gamma_{22}\ell_{21}\\
&\quad + \frac{1}{2}\Big[(q-s)\ell_{21} - s\frac{\ell_{21}}{\ell_{11}^2}\Big],\\
D_t\ell_{22} &= -\Gamma_{21}\frac{\ell_{21}\ell_{22}}{\ell_{11}} + \Gamma_{22}\ell_{22}\\
&\quad + \frac{1}{2}\Big[(q-s)\ell_{22} - \frac{s}{\ell_{22}}\left(1+\frac{\ell_{21}^2}{\ell_{11}^2}\right)\Big]. \qquad (5)
\end{aligned}$$

Equation(5) preserves the SPD nature of $\mathcal{C}$ if $\ell_{ii} > 0$, which we enforce [6, 7] by considering the evolution of $\ln(\ell_{ii})$ instead of ℓ_{ii}.

We use the following initial conditions (superscript 0): $\mathcal{C}^0_{\beta\gamma}(\mathbf{x}) = \delta_{\beta\gamma}$ for all $\mathbf{x}$; and $\omega^0(\mathbf{x}) = \nu\big(-4\ \cos(4y) + 10^{-4}\sum_{m_1=0,m_2=0}^{2,2}[\sin(m_1x+m_2y) + \cos(m_1x+m_2y)]m_2^2/\sqrt{(m_1^2+m_2^2)}\ \big)$. We maintain a constant energy-injection rate $E_{inj} \equiv < F_u \cdot \mathbf{u} >$ by a rescaling of the amplitude F_0 at every time step. Given a value of E_{inj}, the system attains a nonequilibrium, statistically steady state after $\simeq 2-3\tau_e$, where the box-size eddy-turnover time $\tau_e \equiv \mathbb{L}/u_{rms}$ and u_{rms} is the root-mean-square velocity.

In addition to $\boldsymbol{\omega}(\mathbf{x},t)$, $\psi(\mathbf{x},t)$ and $\mathcal{C}(\mathbf{x},t)$ we obtain $\mathbf{u}(\mathbf{x},\mathbf{t})$, the fluid-energy spectrum $E(k) \equiv \sum_{k-1/2<k'\le k+1/2} k'^2\langle|\hat{\psi}(\mathbf{k}',t)|^2\rangle_t$, where $\langle\rangle_t$ denotes a time average over the stastically steady state, the total kinetic energy $\mathcal{E}(t) \equiv \langle\frac{1}{2}|\mathbf{u}(\mathbf{x},\mathbf{t})|^{\mathbf{2}}\rangle_{\mathbf{x}}$, enstrophy $\Omega(t) \equiv \langle\frac{1}{2}|\boldsymbol{\omega}(\mathbf{x},t)|^2\rangle_{\mathbf{x}}$, palinstrophy $\mathcal{P}(t) \equiv \langle\frac{1}{2}|\nabla\times\boldsymbol{\omega}(\mathbf{x},t)|^2\rangle_{\mathbf{x}}$, where $\langle\rangle_{\mathbf{x}}$ denotes an average over our simulation domain, the PDF of scaled polymer extensions $P(r_P/L)$, the PDFs of ω^2, σ^2, and $\Lambda^2 = (\omega^2-\sigma^2)/8$, where $\sigma^2 \equiv \sum_{ij}\sigma_{ij}\sigma_{ij}$, and $\sigma_{ij} \equiv \partial_i u_j + \partial_j u_i$, the PDF of the Cartesian components of u, and the joint PDF of Λ and r_P^2. We obtain the order-p, longitudinal, velocity structure function $S_p(r)$ as follows: We first subtract the mean flow from the velocity field, $\mathbf{u}' = \mathbf{u} - \langle\mathbf{u}\rangle_{\mathbf{t}}$, then we define $\mathcal{S}_p(\mathbf{r}) = \langle\{[\mathbf{u}'(\mathbf{r_c}+\mathbf{r},\mathbf{t}) - \mathbf{u}'(\mathbf{r_c},\mathbf{t})]\cdot\mathbf{r}/r\}^{\mathbf{p}}\rangle_{\mathbf{r_c}}$, where $\mathbf{r}$ has magnitude r and $\mathbf{r_c}$ is an origin, and $\langle\rangle_{\mathbf{r_c}}$ denotes an average over time and the origin (we use $\mathbf{r_c} = (i,j), 2 < i,j < 5$). We then extract the isotropic part $S_p(r)$, by using an SO(2) decomposition [9, 10], by integration over the angle θ that $\mathbf{r}$ makes with the x axis, i.e., $S_p(r) \equiv \int_0^{2\pi}\mathcal{S}_p(\mathbf{r})d\theta$. We concentrate on $S_2(r)$ and the hyperflatness $F_6(r) \equiv S_6(r)/(S_2(r))^3$; the latter provides a convenient measure of the intermittency at the scale r.

In Fig.(1a) we show how the total kinetic energy $\mathcal{E}(t)$ (top panel), enstrophy $\Omega(t)$ (middle panel), and palinstrophy $\mathcal{P}(t)$ (bottom panel) of the fluid fluctuate about their mean values $\langle\mathcal{E}(t)\rangle_{\mathbf{x}}$, $\langle\Omega(t)\rangle_{\mathbf{x}}$, and $\langle\mathcal{P}(t)\rangle_{\mathbf{x}}$ as a function of time t for $c = 0$ (pure fluid) and 0.4. Clearly $\langle\mathcal{E}(t)\rangle_{\mathbf{x}}$, $\langle\Omega(t)\rangle_{\mathbf{x}}$, and $\langle\mathcal{P}(t)\rangle_{\mathbf{x}}$ decrease as c increases. This suggests that the addition of polymers increases the effective viscosity of the solution. However, this naïve conclusion has to be refined because the effective viscosity, bacause of the polymers, depends on the length scale [6, 7] as can be seen by comparing the fluid-energy spectra, with and without polymers, in Fig.(1b). Indeed we can define [6, 7] the effective, scale-dependent viscosity $\nu_e(k) \equiv \nu + \Delta\nu(k)$, with $\Delta\nu(k) \equiv -\mu\sum_{k-1/2<k'\le k+1/2}\mathbf{u}_{\mathbf{k}'}\cdot(\nabla\cdot\mathcal{J})_{-\mathbf{k}'}/[\tau_P k'^2 E^{p,m}(k')]$ and $(\nabla\cdot\mathcal{J})_{\mathbf{k}}$ the Fourier transform of $\nabla\cdot\mathcal{J}$. The right inset of Fig.(2a) shows that $\Delta\nu(k) > 0$ for $k < 30$, where $E^p(k) < E^f(k)$, whereas, for large values of k, $\Delta\nu(k) < 0$, where $E^p(k) > E^f(k)$; the superscripts f and p stand, respectively, for the fluid without and with polymers. The left inset of Fig.(2a) shows the suppression, by polymer additives, of $\Pi(k) = \int_{k'}^{\infty}T(k')dk'$, where $T(k) = \int\hat{u}_i(\mathbf{k})P_{ij}(\mathbf{k})\widehat{(\mathbf{u}\times\boldsymbol{\omega})}_j(\mathbf{k})d\Omega$ and the projector $P_{ij}(k) = \delta_{ij} - \frac{k_i k_j}{k^2}$. The suppression of the spectrum in the small-k regime, which has also been seen in the experiments [11], and preliminary results in Fig. (4.12) of [12], signifies a reduction of the inverse cascade; the enhancement of the spectrum in the large-k regime leads to the reduction in Ω and $\mathcal{P}$ on the addition of polymers (see the middle and bottom panels of Fig.(1a)).

The second-order structure function $S_2(r)$ is related

simply to the energy spectrum. It is natural to ask, therefore, how $S_2(r)$ is modified by the addition of polymers. In Fig(1c), we plot $S_2(r)$ versus r for $c = 0$ (blue circles and run R9) and $c = 0.2$ (green asterisks and run R9); the dashed line, which is shown to guide the eyes has a slope 2; this value is consistent with the $S_2(r) \sim r^2$ form that we expect, at small r, by Taylor expansion. At large values of r, $S_2(r)$ deviates from this r^2 behavior, more so for $c = 0.2$ than for $c = 0$; this is consistence with the results of the experiments of Ref. [13]. The inset of Fig. (1c), which contains plots of the hyperflatness $F_6(r)$ versus r for $c = 0$ (blue circles) and $c = 0.2$ (green asterisks), shows that, on the addition of polymers, small-scale intermittency decreases as c increases. In Fig. (2a), we show how $E^p(k)$ changes, as we increase c : at low and intermediate values of k (e.g., $k = 1$ and 30, respectively), $E^p(k)$ decreases as c increases; but for large values of k (e.g., $k = 100$) it increases with c. Figure (2b) shows how $E^p(k)$ changes, as we increase τ_P with c held fixed at 0.1. At low values of k (e.g., $k = 1$), $E^p(k)$ decreases as τ_P increases; but for large values of k (e.g., $k = 100$) it increases with τ_P. In Fig. (2c) we give plots, for $c = 0.1$, of the spectra $E^p(k)$ for $L = 100$ (red triangles and run R8) and $L = 10$ (green asterisks and run R9); for comparison we also plotc $E^f(k)$ for $c = 0$; as L increases, the difference between $E^p(k)$ and $E^f(k)$ increases at large values of k.

We turn now to the PDF $P(r_p/L)$, which we plot versus the scaled polymer extension r_P/L in Fig. (2d) for $c = 0.1$ and $L = 100$ (red triangles and run R8), $c = 0.4$ and $L = 100$ (black squares and run R8), and $c = 0.1$ and $L = 10$ (green asterisks and run R9). These PDFs fall off sharply (a) near $r_P/L \simeq 1$, because $r_P \leqslant L$, and (b) $r_P \geqslant \sqrt{2}$, because $r_P^2 = \mathrm{Tr}(\mathcal{C}) \geqslant 2$; at values of r_P/L that lie between these two extremes, $P(r_p/L)$ shows a distinct, power-law regime, with an exponent that depends on c, L, and $\mathcal{W}e$; as $\mathcal{W}e$ increases, this power can go from a negative value to a positive value thus signalling a coil-stretch transition. We will give a detailed study of the L and τ_P dependence of $P(r_P/L)$ elsewhere. Here we show a representative plot, for $L = 6$ and $c = 0.1$ (brown dots and run R1), of $P(r_P/L)$ for a case in which the polymers are very nearly stretched.

In Figs. (3a), (3b), and (3c) we show PDFs of Λ, σ^2, and ω^2, respectively, for $c = 0$ (blue circles and run R7) and $c = 0.2$ (red triangles and run R7). These PDFs show that the addition of polymers suppresses large values of Λ, σ^2, and ω^2. The inset of Fig. (3a) shows a filled contour plot of the joint PDF of r_P^2 and Λ; this illustrates that r_P^2 is large where Λ is large and negative, i.e., polymer stretching occurs predominantly in strain-dominated regions; this is evident very strikingly in Fig.(3d), which contains a superimposition of contours of r_P^2 on a pseudocolor plot of Λ; we give a video of a sequence of such plots at *youtube* and at *rahul* .

Our extensive DNS study of two-dimensional fluid turbulence with polymer additives yields good qualitative agreements in low-k regime, with the fluid-energy spectra of Ref. [11] and the second-order velocity structure function of Ref. [13]. In addition, our study brings out new results that we hope will stimulate new experiments. In particular, experiments should be able to measure (a) the reduction of $\langle \mathcal{E}(t) \rangle_{\mathbf{x}}$, $\langle \Omega(t) \rangle_{\mathbf{x}}$, and $\langle \mathcal{P}(t) \rangle_{\mathbf{x}}$ shown in Fig. (1a), (b) the modification of $E^p(k)$ at large k (Fig. (1b)), (c) the c and L dependence of $E^p k$ illustrated in Figs. (2a)-(2c), (d) the PDF of (r_P/L), Λ, σ^2, and ω^2, and (e) the stretching of polymers in strain-dominated regions as illustrated in Fig. (3d).

We thank D. Mitra for discussions, CSIR, UGC, DST (India), and the COST Action MP0806 for support, and SERC (IISc) for computational resources. PP and RP are members of the International Collaboration for Turbulence Research.

* anupam@physics.iisc.ernet.in
† p.perlekar@tue.nl
‡ rahul@physics.iisc.ernet.in;
also at Jawaharlal Nehru Centre For Advanced Scientific Research, Jakkur, Bangalore, India.

[1] B.A. Toms, in Proceedings of the International Congress on Rheology (North-Holland, Amsterdam, 1949); J. Lumley, J. Polym. Sci **7**, 263 (1973).
[2] P. Virk, AIChE **21**, 625 (1975).
[3] J.W. Hoyt, Trans. ASME J. Basic Eng. 94:25885 (1972).
[4] E. van Doorn, C.M. White, and K.R. Sreenivasan, Phys. Fluids **11**, 2387 (1999).
[5] C. Kalelkar, R. Govindarajan, and R. Pandit, Phys. Rev. E **72**, 017301 (2004).
[6] P. Perlekar, D. Mitra, and R. Pandit, Phys. Rev. Lett. **97**, 264501 (2006).
[7] P. Perlekar, D. Mitra, and R. Pandit, Phys. Rev. E. **82**, 066313 (2010).
[8] N. Ouellette, H. Xu, and E. Bodenschatz, J. Fluid Mech. **629**, 375 (2009); A.M Crawford, N. Mordant, H. Xu and E. Bodenschatz, New Journal of Physics **10** (2008) 123015.
[9] E. Bouchbinder, I. Procaccia, and S. Sela, Phys. Rev. Lett. **95**, 255503 (2005).
[10] P. Perlekar, and R. Pandit, New Journal of Physics, 614 11, 073003 (2009).
[11] Y. Amarouchene and H. Kellay, Phys. Rev. Lett. **89**, 104502 (2002).
[12] S. Musacchio, Ph.D. thesis, Department of Physics, Turin University, 2003.
[13] Y. Jun, J. Zhang, and X-L Wu, Phys. Rev. Lett. **96**, 024502 (2006).
[14] G. Boffetta, A. Celani, and A. Mazzino, Phys. Rev. Lett. **91**, 034501 (2003); Phys. Rev. E **71**, 036307 (2005); S. Berti and G. Boffetta, Phys. Rev. E **82**, 036314 (2010).
[15] AB Okubo, Deep-Sea. Res. **17** 445 (1970); J. Weiss, Physica D **48**, 273 (1992).
[16] G. Boffetta and R. Ecke, Annu Rev Fluid Mech. **44**, 427-451 (2012); R. Pandit, P. Perlekar, and S. S. Ray, Pramana-Journal of Physics,**73**, 157(2009).

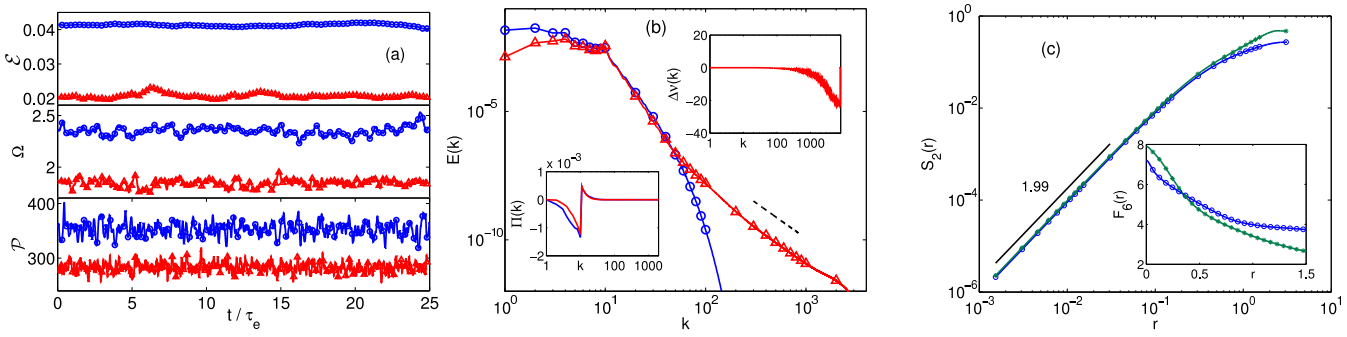

FIG. 1. (Color online) (a) Plots versus time t/τ_e for run R7 of the total kinetic energy of the fluid $\mathcal{E}$ (top panel), the enstrophy Ω (middle panel),and the palinstrophy $\mathcal{P}$ (bottom panel) for $c = 0$ (blue circles) and $c = 0.4$ (black square); (b)Log-log (base 10) plots of the energy spectra $E(k)$ versus k for $c = 0.2$ (red triangles) and $c = 0$ (blue circles); left inset: energy flux $\Pi(k)$ versus k for $c = 0.2$ (red line) and $c = 0$ (blue line); right inset: polymer contribution to the scale-dependent viscosity $\Delta\nu(k)$ versus k for $c = 0.2$ (blue line) for runs R10; bottom (c) Plots of the second order velocity structure function $S_2(r)$ versus r versus run R7 for $c = 0$ (blue circle) and $c = 0.2$ (red triangles); the dashed line with slope 1.98 is shown for comparision; the inset shows a plot of the hyperflatness $F_6(r)$ versus for r for $c = 0$ (blue circles) and $c = 0.2$ (red triangles).

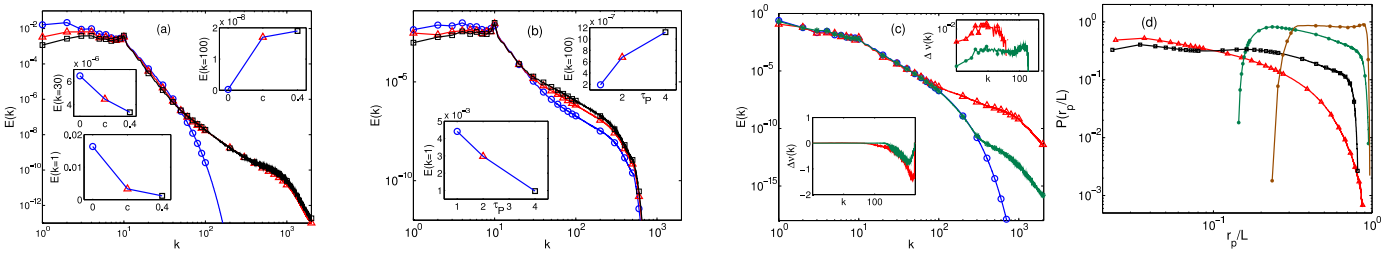

FIG. 2. (Color online) (a) Log-log (base 10) plots of the energy spectra $E(k)$ versus k for $c = 0$ (bluecircles), for $c = 0.2$ (red triangles) and $c = 0.4$ (black squares); left bottom inset: variation of $E(k)$ with polymer concentration for $\tau_P = 1$ and $k = 1$; left up inset: variation of $E(k)$ with polymer concentration for $\tau_P = 1$ and $k = 30$; right up inset: variation of $E(k)$ with polymer concentration for $\tau_P = 1$ and $k = 100$; run R7; (b) Log-log (base 10) plots of the energy spectra $E(k)$ versus k for $\tau_P = 1$ (blue line with open circles) , for $\tau_P = 0.2$ (red line with open triangles) and $\tau_P = 4$ (black line with open squares); left bottom inset: variation of $E(k)$ with polymer relaxation time for $c = 0.4$ and $k = 1$; right up inset: variation of $E(k)$ with polymer relaxation time fot $c = 0.4$ and $k = 100$; run R2 (c) Log-log (base 10) plots, for $c = 0.2$ and $\tau_P = 1$, of the energy spectra $E(k)$ versus k for $L = 100$ (red triangles) and $L = 10$ (green asterisks); for comparison we put $c = 0.0$ (blue circles); left bottom inset: $\Delta\nu(k)$ versus k; right up inset: zoomed picutre of the above said inset, (d) PDFs of polymer extensions $P(r_P^2/L^2)$ versus r_P^2/L^2 for $c = 0.2$ (red triangles), $c = 0.4$ (black squares) for run R8, $c = 0.2$ and $L = 10$ (green asterisks) for run R9, and $c = 0.2$ and $L = 6$ (brown dots) for run R1

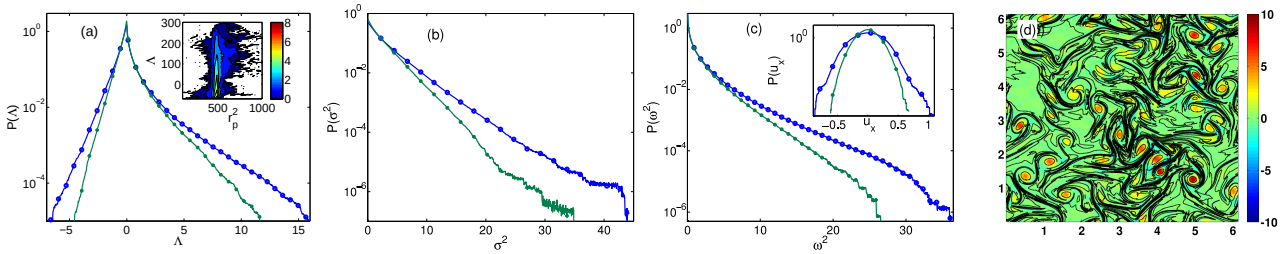

FIG. 3. (Color online) Probability distribution function (PDFs) of (a) the Okubo-Weiss parameter Λ for run R7; the inset shows a filled contour plot of the joint PDF of Λ and r_P^2, the square of the polymer extension; (b) σ^2, the square of the strain rate, for run R7, and (c) ω^2, the square of the vorticity, the inset is PDF of scaled polymer extensions (r_P/L); for $c = 0$ (blue circles) and $c = 0.2$ (red triangles) for run R7 (d) A representative pseudocolor plot of Λ superimposed on a contour plot of r_P^2 run R10.

	N	L	τ_P	$\delta t \times 10^4$	E_{inj}	$\nu \times 10^{-4}$	$\mathcal{W}e$	c	Re_λ	$k_{max}\eta_d$
R1	512	6	2	10.0	0.008	10.0	4.40	0.1	107, 85	3.4, 3.6
R2	1024	100	1, 2, 4	1.0	0.005	5.0	2.11 4.02 6.01	0.1	221, 121, 95 , 68	5.1, 5.3, 5.4, 5.5
R3	2048	100	1	1.0	0.003	5.0	1.60	0.4	147, 60	14.1, 14.8
R4	2048	100	1	1.0	0.0015	5.0	1.26	0.2	86 , 54	13.2, 13.6
R5	4096	100	1	1.0	0.005	5.0	2.08	0.2	233, 90	20.2, 20.9
R6	4096	100	1	1.0	0.002	5.0	2.08	0.2 0.4	108, 62, 45	24.8, 25.8, 26.2
R7	4096	10	1	1.0	0.002	5.0	2.08	0.4	108, 90	24.8, 26.2
R8	4096	100	1	0.5	0.005	1.0	2.81	0.1	1451, 1407	8.0, 8.2
R9	4096	10	1	0.5	0.005	1.0	2.81	0.1	1451, 1407	8.0, 8.2
R10	16384	100	1	0.5	0.002	5.0	1.40	0.2	105, 60	96.4, 102.7

TABLE I. The parameters for our DNS runs R1-R10 for the two-dimensional, incompressible Navier-Stokes equation with air-drag-induced friction and polymer additives modelled via the FENE-P model. In all our runs the polymer relaxation time $\tau_P = 1.0$ and the friction coefficient $\alpha = 0.01$. We also carry out DNS studies of the two-dimensional NS equation with the same numerical resolutions as used in our runs with polymer additives. N is the number of collocation points, δt the time step, E_{inj} the energy-injection rate, ν the kinematic viscosity, and c the concentration parameter. The Taylor-microscale Reynolds number is $Re_\lambda \equiv \sqrt{2}\mathcal{E}/\sqrt{\nu\epsilon}$ and the Weissenberg number is $We \equiv \tau_P\sqrt{\epsilon/\nu}$, where $\mathcal{E}$ is the total kinetic energy of the fluid and ϵ the energy dissipation rate per unit mass for the fluid.

[17] A. Kurganov and E. Tadmor, J. Comput. Phys. **160**, 241282 (2000).
[18] T. Vaithianathan and L. Collins, J. Comput. Phys. **187**, 1 (2003).
[19] http://www.fftw.org